

Topological Analysis of Linear Polymer Melts

Christos Tzoumanekas* and Doros N. Theodorou†

*Department of Materials Science and Engineering, School of Chemical Engineering,
National Technical University of Athens, Zografou Campus, 15780 Athens, Greece and
Dutch Polymer Institute (DPI), The Netherlands*

(Dated: 14th September 2018)

We introduce an algorithm for the reduction of computer generated atomistic polymer samples to networks of primitive paths. By examining network ensembles of Polyethylene and cis-1,4 Polybutadiene melts, we quantify the underlying topologies through the radial distribution function of entanglements and the distribution of the number of monomers between entanglements. A suitable scaling of acquired data leads to a unifying microscopic topological description of both melts.

Polymer chains cannot cross each other. A successful conceptual framework embodying this principle at the molecular level is offered by the tube model [1, 2]. The tube model postulates that the mutual uncrossability of polymer chains generates topological constraints (TCs), referred to as entanglements, which effectively restrict individual chain conformations in a curvilinear tube-like region enclosing each chain. Lateral chain motion is confined to the length scale of the tube diameter. Large-scale motion is promoted via reptation [1], an effective one-dimensional diffusion of a chain along its tube axis. The latter provides a coarse-grained representation that characterizes the chain topology and is called the Primitive Path (PP). Edwards [3] regarded the PP as the shortest path constructed by keeping the chain ends fixed while continuously tightening (shrinking) the chain contour, so that the resulting path has the same topology relative to other chains as the chain itself [2, 3]. Applying this construction for all chains [4, 5] leads to a coarse-grained picture of a polymer melt that uncovers its large-scale *topological substructure*. The latter is conceived as a network of entangled PPs underlying the melt structure [6]. The tube diameter d is assumed uniform and corresponds to the mesh length of this network [2].

Entanglements dominate the rheological and dynamical properties of large-molecular weight polymer melts [2], as well as the ultimate mechanical properties in the glassy state of these systems [7]. Their topological nature makes their direct experimental study difficult and their microscopic definition elusive [8]. In this letter, we present *microscopically determined distributions* that describe in a statistical manner the topological state of flexible polymer melts. We utilize an algorithm, referred to as CReTA (Contour Reduction Topological Analysis), which is capable of reducing the atomistic configuration of a computational polymer sample to a network of corresponding PPs. Nodal points of the reduced network correspond to TCs experienced by individual chains, while network connectivity defines the underlying melt topology. Topological measures extracted from networks of entangled Polyethylene (PE) and cis-1,4 Polybutadiene (PB) melts are compared against corresponding experimental data. Quantitative agreement establishes these

networks as meaningful, well defined, structural representations of the underlying melt topologies.

Mesoscopic views where a polymer melt is represented as an entanglement network (rubber analogy) have long been used as conceptual abstractions for the development of phenomenological models (transient network theory), and analytical theories (tube model) in polymer physics. These views are guided from the rubber-like response of melts in viscoelastic experiments (rubbery plateau in the relaxation modulus), and the Random Walk (RW) statistics underlying the structure of flexible polymers. RW-like chain configurations, above some length scale show a self-similarity, to which universalities and scaling laws detectable in physical properties can be traced. Here, by examining networks generated from well packed RW-like chain configurations of chemically different polymer melts, we characterize the melt topology through *distributions* which, when scaled accordingly, unveil a *unifying topological description*. The reported statistical properties of entanglement networks constitute a *missing link* for the construction of mesoscopic simulation models of polymer melts [6] and glasses [9] suitable for the prediction of rheological and large-deformation mechanical properties. One can use PP statistics in reverse-engineering fashion to construct entanglement networks obeying the mentioned distributions, for any flexible polymer. Microscopically determined PPs offer a promising basis [5, 10, 11] for investigating the general picture of entanglements invoked by the tube model.

Following Edwards's perspective and as proposed in [4, 5], CReTA provides a solution to the following geometric problem [11]: 'Given a set of uncrossable curved lines in space, reduce continuously their contour lengths keeping their ends fixed, until they become sets of rectilinear segments (entanglement strands) coming together at nodal points (entanglements)'. For each polymer we examine an ensemble of statistically independent atomistic samples. The ensembles have been thermodynamically and topologically equilibrated at all length scales by previous Monte Carlo simulations [13, 14] employing chain-connectivity altering moves which alter the system topology. Through CReTA, atomistic configurations are transformed to networks, which are then analyzed to ex-

tract topological properties.

CReTA implements random aligning string moves and hardcore interactions. CH_x monomers are treated as united-atom hard spheres of diameter σ . Chains are represented as series of fused spheres, since in atomistic polymer models the skeletal bond distance ($\sim 1.5\text{\AA}$) is lower than σ ($\sim 3.5\text{\AA}$). Periodic boundary conditions apply in all cubic sample directions. A string is defined as a set of $m \geq 1$ consecutive chain atoms. On each move, a string is randomly chosen and the string atoms are displaced to corresponding equidistant points on the straight line segment joining the atoms on either side of the string. Chain ends are fixed throughout the process. To avoid chain crossing and preserve system topology, moves leading to overlaps between any string atom with any other atom belonging to a different chain are rejected. This is sufficient for preventing crossing when chains consist of fused spheres. m is randomly chosen from an interval of $\Delta m \sim 10$ width. Accepted moves result in simultaneous reduction of chain contours and progressive shrinkage of unentangled loops to straight strands composed of fused spheres. Rejected moves stem from either mutually blocked chain parts, which will lead to entanglements, or from contacts between unentangled loops, which will eventually disappear. To accelerate chain tightening we increase string sizes by gradually increasing Δm . When chain contour lengths are no longer diminishing, chain thickness is reduced by decreasing σ and the process starts anew. This aids in tightening meshed unentangled loops, which, although temporarily blocked, do not represent true TCs. Upon decreasing σ , to preserve the fused sphere sequence of chains we place an auxiliary atom between successive skeletal atoms that have lost contact. Auxiliary atoms are excluded from latter analysis. The whole procedure terminates when a predefined $\sigma_f \sim 0.5\text{\AA}$ is reached. At this point an underlying network structure of interpenetrating ‘zigzag’ shaped PPs has been revealed [15]. Further σ reduction to attain the infinitely-thin-continuous line limit would be time consuming and superfluous. CReTA differs from recent similar approaches. In [5], contour reduction is achieved through the minimization of an elastic energy which does not lead to well defined networks of ‘kinky’ PPs where nodal points can be specified. Kröger’s approach [11] is also geometric and capable of generating networks but, unlike CReTA, cannot track a monomer in the system both in the melt and network configurations. The latter feature offers great potential for studying hidden topological correlations in space, time, and along the chains, in close connection with the melt structure and dynamics. The $P(n)$ distribution presented later is an example of this.

As shown in Fig. 1, the resulting PPs consist of short pairwise blocked chain sections connected by straight strands of fused atoms. By examining blocked regions we resolve PP ‘contacts’ to pairs of neighboring monomers.

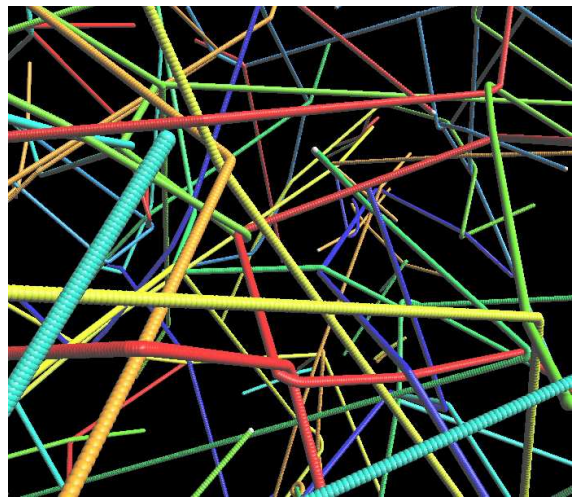


Figure 1: (color online). PP network view of a PE melt.

These specify pairwise associated TCs in the monomer sequence of their parent chains. In addition, they represent effective spatial localization points of the TCs each chain is subjected to. By convention, we refer to these points as entanglements. Each PP is characterized by its ends and a set of entanglements with specific spatial locations, monomer sequence indices, and pairwise associations to other entanglements. The whole structure is reduced to a network, with nodal points the entanglements, and edges the joining entanglement strands (ESs). *Topological analysis* reduces then to an examination of network properties. Entanglement spacing (network mesh) on the PP contour is deduced both in monomer and length units by calculating \overline{N}_{ES} and \overline{d}_{ES} , the ensemble average number of monomers and end-to-end length, respectively, of an ES. Experimentally, entanglement spacing is mainly inferred either from the ES monomer length N_e , measured from the plateau regime of the dynamic shear modulus [12], or from the tube diameter d (entanglement distance) measured as an intermediate dynamic length in neutron spin echo studies of the dynamic structure factor [8]. These are interpreted on the basis of the tube model, where PP conformations are considered as RWs and an ES is identified with the PP Kuhn segment [2]. Here, the relevant quantities are the PP Kuhn length $d = R^2/L$, and the number of monomers in a PP Kuhn segment $N_e = NR^2/L^2$. N denotes the chain average number of monomers. R^2 and L are the PP squared end-to-end distance and contour length, respectively, calculated here as ensemble averages. By this ‘Kuhn mapping’ approach, entanglement spacing emerges as the mesh spacing of an assumed uniform PP network of interpenetrating random walks.

Table I summarizes our results for \overline{N}_{ES} , N_e , \overline{d}_{ES} , d , the packing length p and the density of the atomistic samples, along with corresponding experimental values.

Table I: Entanglement spacing in monomer (\bar{N}_{ES} , N_e), and length (\bar{d}_{ES} , d) units of PP networks, and packing length p of the initial atomistic samples (equilibrated at $T = 450\text{K}$ (PE), $T = 413\text{K}$ (PB)). \bar{N}_{ES} , \bar{d}_{ES} refer to the natural network mesh. N_e , d refer to the PP Kuhn mapping approach. Numbers in parentheses are experimental values from [12], unless otherwise indicated. The calculated polymer densities are $0.776(0.766)^a$, $0.778(0.766)^a$, $0.867(0.826)$ g/cm^3 ; the polydispersity indices are 1.083, 1.000, 1.053; and the number of chains for each system studied are 16, 8, 24 (top to bottom).

	N	\bar{N}_{ES}	\bar{d}_{ES} (Å)	N_e	d (Å)	p (Å)
PE 500	500	28.3	14.0	75.1(61.4)	38.4(39.8) ^b	1.53(1.69)
PE 1000	1000	29.1	14.1	74.2(61.4)	36.6(39.8) ^b	1.65(1.69)
PB 1000	1000	80.9	18.7	178.7(173.8)	42.3(43.0)	2.59(2.44)

^aRef. 16.

^bRef. 8.

p , an effective chain thickness that controls coil packing, is defined as $1/(\rho_{ch}R^2)$, where ρ_{ch} is the number density of chains. Volumetric, structural and conformational predictions for both polymers [13, 14] are in excellent agreement with available experimental data. From the additional p data presented here, we conclude that the interplay between large-scale chain conformation and monomer packing is nicely captured by the atomistic ensembles. Turning to networks, PE samples of $N = 500, 1000$ display practically the same mesh values, showing that well entangled samples possess a *quantitatively* similar underlying topology, independently of chain length. The small differences are attributed to different packing lengths. \bar{N}_{ES} , \bar{d}_{ES} , the network natural mesh spacing quantities, are much smaller than the corresponding PP Kuhn segment quantities N_e , d , with $\bar{N}_{ES} \sim 0.4N_e$ for both materials. This happens because of directional correlations between ESs in the same PP that decay exponentially with ES separation. That is, PP conformations are not RWs, and PP Kuhn segments are not free of TCs. At the Kuhn scale, where PPs become RWs, N_e , d for both polymers are in good agreement with experimental data. If we consider our systems as rubber networks, however, the small value of \bar{N}_{ES} implies a larger plateau modulus G_o than found experimentally. Interestingly, in recent [6] Brownian dynamics simulations of 3D PP networks, the linear viscoelastic response of PB solutions is reproduced quantitatively only when an N_e of about half the experimental value is utilized, as found here for \bar{N}_{ES} . The discrepancy is attributed [6] to the affine as opposed to phantom network model experimental estimate of G_o . In this respect, our results are in favor of the phantom model, which for a tetrafunctional network would estimate approximately half an N_e for the same G_o [6].

In Fig. 2 we present the *normalized* distribution $P(n)$

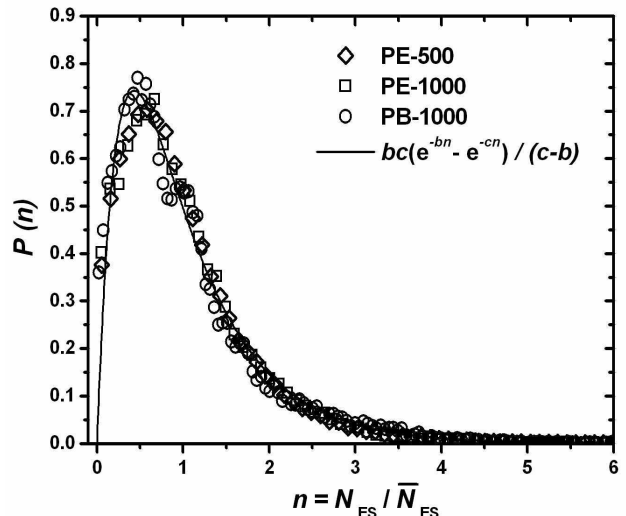


Figure 2: Normalized distribution of the reduced monomer distance between entanglements for the polymers of Table I.

of the reduced number of monomers N_{ES} in an ES, $n = N_{ES}/\bar{N}_{ES}$. The data from both materials superimpose on each other, falling on a master curve of the form $P(n) = \frac{bc}{c-b}(e^{-bn} - e^{-cn})$, with fitted values $b = 1.30$, $c = 3.78$. In view of the large difference in \bar{N}_{ES} , p between PE and PB, the collapse of data suggests a universal character of $P(n)$ for linear polymers. The distribution is very broad with an exponential tail and in contrast with the tube model implies a non-uniform network mesh and large fluctuations in the number of monomers of an ES. The origin of such fluctuations [4] and their effect on rheological properties have recently been examined [17, 18]. Schieber [18] considered a Gaussian chain with a constant number of Kuhn segments in contact with a ‘bath’ of entanglements. By fixing the corresponding chemical potential, he came up with an exponential distribution for the number of Kuhn segments in an ES. Stochastically, this distribution can be generated [18] by marching from one chain end to the other and placing entanglements on Kuhn segments according to a Poisson process [19] of ‘entanglement events’. In our case the exponential tail of $P(n)$ is the result of a similar stochastic process evolving on the *monomer sequence space* of a chain (see below). However, in a Poisson process successive events can come arbitrarily close, while it is meaningful to assume that an entanglement requires a certain number of successive monomers to develop. This creates an *effective repulsion* between successive entanglements in the monomer sequence space of a chain, which will become prominent close to and below the number of monomers of the Kuhn segment of the atomistic chain. This is evidenced in Fig. 2 by the downturn and vanishing trend of $P(n)$ data as $n \rightarrow 0$.

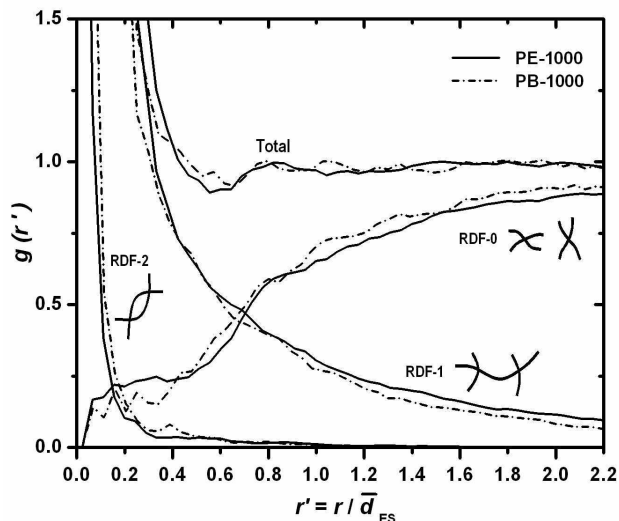


Figure 3: Total and partial RDFs of PE-1000 (solid) and PB-1000 (dashed). Partial RDFs depict correlations between different pair types of binary entanglements. RDF-0 curves correspond to entanglements that are ‘*spatial neighbors*’, i.e., all four chains passing through them are different. RDF-1, RDF-2 curves correspond to entanglements at *any distance* that are ‘*topological neighbors*’, i.e., connected by one or two common chains, respectively, passing through them. Each case is sketched in the figure.

A *stochastic interpretation* of our results can be given in terms of a *renewal process* [19], which is the generalization of a Poisson process. In such a process, successive events are still identically, independently distributed, though with a distribution that is not exponential, cf. the normalized $P(n)$ presented here. Moreover, $P(n)$ is the convolution of two exponential distributions, namely be^{-bn} and ce^{-cn} , and can be interpreted [19] as the result of two (uncorrelated) alternating Poisson processes with rates b , c , evolving on *the monomer sequence space* of a chain. The first process, with rate c , does not result in observable events [19]. What it does is to stochastically create an unentangled monomer sequence in front of an entanglement, corresponding to the mentioned repulsion. The second process, with rate b , takes over when an unentangled sequence has been created and places an entanglement in one of the following monomers.

Finally, in Fig. 3 we present the total and partial radial distribution functions (RDFs) of entanglements versus $r' = r/\bar{d}_{ES}$, the spatial distance r reduced by the average network mesh length. Apart from some minor differences, the curves for PE, PB superimpose on each other. Therefore, the spatial network nodal correlations stemming from the underlying topologies of the PE, PB melts are similar when scaled accordingly. The presence of very small network strands, which connect first topological neighbors (see Fig. 3), is responsible for the

effective *spatial attraction* evidenced in the total RDF for $r' \lesssim 0.4$, and separately in RDF-1,2. The fact that RDF-0 curves are below RDF-1 curves for $r' \lesssim 0.7$ indicates that in the region around and near an entanglement topological neighbors persist and spatial neighbors cannot easily penetrate. The latter populate primarily the region beyond $r' \sim 0.7$ around a network node, where RDF-0 curves overpass RDF-1 curves. RDF-2 curves fall rapidly with r' and correspond to pairs of chains intertwined through two entanglements. Intertwining results in closely spaced entanglements and is highly improbable at large r' . The total RDF implies that in the range $r' \gtrsim 0.8$ the network structure can be described as an *ideal dilute gas* of entanglements [7], with *short range correlations* occurring at smaller r' .

In summary, common organization properties of topological constraints in polymer melts have been revealed through a statistical analysis of primitive paths. We are grateful to N. Karayiannis, V. Mavrantzas and P. Gestoso for providing the atomistic polymer samples. This work is funded by the Dutch Polymer Institute.

* Electronic address: tzoum@central.ntua.gr

† Electronic address: doros@chemeng.ntua.gr

- [1] P.G. de Gennes, *J. Chem. Phys.* **55**, 572 (1971).
- [2] M. Doi and S.F. Edwards, *The Theory of Polymer Dynamics*, (Clarendon, Oxford, 1986).
- [3] S.F. Edwards, *Br. Polym. J.* **9**, 140 (1977).
- [4] M. Rubinstein and E. Helfand, *J. Chem. Phys.* **82**, 2477 (1984).
- [5] S.K. Sukumaran *et al.*, *J. Polym. Sci. Part B: Polym. Phys.* **43**, 917 (2005); R. Everaers *et al.*, *Science* **303**, 823 (2004).
- [6] Y. Masubuchi *et al.*, *J. Chem. Phys.* **119**, 6925 (2003).
- [7] J.J. Benkoski, G.H. Fredrickson, and E.J. Kramer, *J. Polym. Sci. Part B: Polym. Phys.* **40**, 2377 (2002).
- [8] D. Richter *et al.*, *Macromolecules* **26**, 795 (1993).
- [9] Y. Termonia, *Macromolecules* **24**, 1128 (1991); A.F. Terzis, D.N. Theodorou, A. Stroeks, *ibid.* **35**, 508 (2002).
- [10] S. Shanbhag and R.G. Larson, *Phys. Rev. Lett.* **94**, 76001 (2005); Q. Zhou and R.G. Larson, *Macromolecules* **38**, 5761 (2005); R.S. Hoy and M.O. Robbins, *Phys. Rev. E* **72**, 061802 (2005).
- [11] M. Kröger, *Comput. Phys. Commun.* **168**, 209 (2005).
- [12] L.J. Fetters *et al.*, *Macromolecules* **27**, 4639 (1994); L.J. Fetters, D.J. Lohse, and W.W. Graessley, *J. Polym. Sci. Part B: Polym. Phys.* **37**, 1023 (1999).
- [13] N.C. Karayiannis, V.G. Mavrantzas, and D.N. Theodorou, *Phys. Rev. Lett.* **88**, 105503 (2002).
- [14] P. Gestoso *et al.*, *Macromolecules* **36**, 6925, (2003).
- [15] We note that categorizing the chains into subsets and reducing the subsets sequentially in arbitrary order leads practically to the same network structure.
- [16] D.S. Pearson *et al.*, *Macromolecules* **20**, 1137 (1987).
- [17] F. Greco, *Phys. Rev. Lett.* **88**, 108301 (2002).
- [18] J.D. Schieber, *J. Chem. Phys.* **118**, 5162 (2003).
- [19] D.R. Cox, V. Isham, *Point Processes*, (Chapman and Hall, London, 1980).